RSC Advances

PAPER

View Article Online
View Journal | View Issue

Cite this: *RSC Adv.*, 2021, **11**, 30771

Selective and sensitive electrochemical sensors based on an ion imprinting polymer and graphene oxide for the detection of ultra-trace Cd(II) in biological samples†

A. B. Abdallah, *[a] Mohamed R. El-kholany, [a] A. F. S. Molouk,[a] Tamer Awad Ali,[b] A. A. El-Shafei[a] and Magdi E. Khalifa[a]

New selective and sensitive electrochemical sensors were designed based on the deposition of a promising ion imprinted polymer (IIP) on the surface of glassy carbon electrode (GCE) for the detection and monitoring of Cd(II) in different real samples. Herein, a highly selective Cd-imprinted polymer was successfully synthesized using a novel heterocyclic compound based on the benzo[*f*]chromene scaffold that acted as a complexing agent and a functional monomer in the presence of azobisisobutyronitrile (initiator) and ethylene glycol dimethacrylate (cross-linker). The characterization of the synthesized chelating agent and IIP was performed using FT-IR, SEM, ^{1}H-NMR, EIMS, and EDX analyses. After that, the voltammetric sensor was manufactured by introducing graphene oxide (GO) on the surface of GCE; then, the IIP was grown by a drop coating technique. The electrochemical characterization of the voltammetric sensor (IIP/GO@GCE) was performed by CV and EIS. For comparison, the potentiometric sensor was also prepared by embedding IIP in plasticized polyvinyl chloride and depositing it as one layer on the GCE surface. Anodic stripping voltammetry was used to construct the calibration graph; the IIP/GO@GCE exhibited a wider detection range (4.2×10^{-12}–5.6×10^{-3} mol L^{-1}) and extremely low detection limit (7×10^{-14} mol L^{-1}) for Cd(II). Meanwhile, the potentiometric sensor showed a linear calibration curve for Cd(II) over a concentration range from 7.3×10^{-8} mol L^{-1} to 2.4×10^{-3} mol L^{-1} with a detection limit of 6.3×10^{-10} mol L^{-1}. Furthermore, both sensors offered outstanding selectivity for Cd(II) over a wide assortment of other common ions, high reproducibility, and excellent stability.

Received 17th July 2021
Accepted 27th August 2021

DOI: 10.1039/d1ra05489a

rsc.li/rsc-advances

1. Introduction

Cadmium (Cd) is one of the most utilized metals in agriculture and industry, with application such as pigments, electric batteries, nuclear reactors, and electronic components, in addition to various biological interests.[1–3] Despite the widespread use of cadmium, it is considered one of the most detrimental heavy metals for human health. According to the World Health Organization (WHO), the maximum permissible limits of Cd for the human body have been established at 3.0 to 5.0 μg L^{-1}.[4] Therefore, most exposure of humans to Cd from various sources becomes highly toxic for a relatively long time. An excess cadmium induces hepatotoxicity due to increasing liver-related proteins such as nuclear factor erythroid 2-related factor 2 (Nrf2) and Kelch-like ECH-associated protein 1 (Keap1), which are carried to the kidneys and finally lead to kidney failure.[5–7] Furthermore, bioaccumulation of Cd in the human body leads to blood cancer, heart disease, and a series of organ dysfunctions.[6] Therefore, the recognition and determination of cadmium concentration *via* sensitive, selective, and simple analytical methods is essential for health and pollution control. Atomic absorption spectrophotometry, capillary electrophoresis, plasma atomic emission spectrometry, and flame atomic fluorescence spectrometry are the most popular methods for cadmium determination.[8–11] Unfortunately, many of these analytical techniques are not convenient for popular usage due to their long time consumption, and they often require professional operators and costly instruments.[12] Currently, electrochemical techniques (voltammetry, potentiometry, coulometry, *etc.*) are receiving wide attention for the analysis of trace pollutants.[12–14]

Potentiometric methods are classic analytical techniques that measure the electromotive force (EMF) of the cell when no significant current flows between the working and reference electrodes. By comparing with other electro-analytical techniques, this method provides information about the activity of ions or molecules in the electrochemical solution. Moreover,

[a]*Department of Chemistry, Faculty of Science, Mansoura University, El-Gomhoria Street, Mansoura-35516, Egypt. E-mail: ahmed.bahgat@mans.edu.com; Tel: +20 1090433273*

[b]*Egyptian Petroleum Research Institute, 12622, Egypt*

† Electronic supplementary information (ESI) available. See DOI: 10.1039/d1ra05489a

this technique extends to the highly sensitive and selective quantitative determination of different analytes in real samples. Aglan *et al.* and Mashhadizadeh *et al.* modified carbon paste electrode (CPE) with lanthanum tungstate ion exchanger and mercapto-gold nanoparticles, respectively, for the determination of cadmium ions in different real samples using a potentiometric technique.[15,16] The modified sensors exhibited high stability and short response times for cadmium detection. However, the lack of selectivity of the sensors was the major problem faced by authors during the electrochemical determination.

On the other hand, voltammetry belongs to the main category of electro-analytical techniques in which the current is directly or inversely proportional to the concentration of the target analyte based on the variation of the potential.[12] Due to the high sensitivity and excellent selectivity of the voltammetric method, it has been widely used for the determination of organic and/or inorganic species.[17,18] Cyclic voltammetry (CV), differential pulse voltammetry (DPV), square wave voltammetry (SWV) and anodic stripping voltammetry (ASV) are additional voltammetric techniques for the determination of different target analytes. The ASV method is one of the most popular voltammetric techniques for recognition and detection of up to thirty different elements.[15,17–20] Due to the capability of ASV to concentrate the metal analyte over the working electrode surface at a high negative potential before the electrochemical determination, it is used for quantification of low concentration levels of analytes. After the preconcentration step, dissolution of the deposited metals is achieved by sweeping the potential in the anodic direction. Despite the high sensitivity of this technique, it still suffers from the deficiency of selectivity. Therefore, an ion imprinting polymer (IIP) is used to enhance the selectivity of the working electrode.[12] The ion imprinting technique is a versatile approach for synthesizing a polymer matrix with a high affinity for a template ion that is chosen depending on the polymerization process.[17,18] The IIP is usually fabricated by the polymerization of monomers with a cross-linker in the presence of an initiator and the template ion. Then, after leaching of target ions, imprinted cavities are formed in the polymeric matrices.[21–23] Despite the great attention that has been paid to imprinted sensors, there are intrinsic difficulties in their practical application due to the sluggish direct electron transfer. Therefore, to improve the responses of these sensors, researchers have utilized different electrocatalytic nanomaterials (graphene oxide, gold nanoparticles, multi-walled carbon nanotubes, *etc.*).[22,23] Graphene oxide (GO) is a fascinating scientific material due to its unique surface nature, which enhances its mechanical and thermal stability, electrical conductivity, and molecular barrier abilities.[12]

A literature survey has reported various modified working electrodes (*e.g.* glassy carbon electrode (GCE), carbon paste electrode (CPE), and gold electrode) for the detection of Cd(II) based on different IIPs and some nanomaterials. However, most of these electrodes are not suitable for *in situ* analysis due to some issues, such as storage stability and problems associated with the interference of cadmium ion analogues (Table S1, ESI†). In this respect, many researchers worldwide are paying growing attention to the design and development of stable and selective electrodes for cadmium detection in real samples by voltammetric and potentiometric techniques. In this work, ethyl 6-(allyloxy)-2-amino-4-phenyl-4*H*-benzo[*f*]chromene-3-carboxylate (EAAP) (**2**) is a new complexing agent and a functional monomer that was used for the preparation of a Cd(II)-imprinted polymer in the presence of azobisisobutyronitrile (AIBN, initiator) and ethylene glycol dimethacrylate (EGDMA, cross-linker). Full characterization of the ligand and the prepared IIP was performed using proton nuclear magnetic resonance (^{1}H NMR) spectroscopy, Fourier-transform infrared (FT-IR) spectroscopy, scanning electron microscopy (SEM), electron impact mass spectroscopy (EIMS) and energy-dispersive X-ray (EDX) spectroscopy. For the electrochemical application, the GCE (electrochemical transducer) was modified with the prepared IIP in the presence of graphene oxide (GO) for voltammetric measurements. In contrast, the IIP was deposited on the surface of the GCE after embedding it in a plasticized polyvinyl chloride (PVC) membrane to form the potentiometric sensor. The effects of different factors on the proposed sensors' responses was elaborated to optimize the conditions of the electrochemical experiment. Also, the voltammetric and potentiometric sensors were successfully used to detect trace Cd(II) concentrations in different real samples.

2. Experimental section

2.1 Chemicals and reagents

All the chemicals and reagents in this work were used without further purification, and their solutions were prepared using double distilled water. Natural graphite powder (1–2 μm), dimethylformamide (DMF, 99.8%), ethanol (EtOH), cadmium chloride, glacial acetic acid, sodium acetate, 2,7-dihydroxynaphthalene, allyl bromide and EGDMA were obtained from Sigma-Aldrich. High molecular weight polyvinyl chloride (PVC) powder, nitric acid (70%), potassium ferrocyanide, potassium ferricyanide, dioctyl phthalate (DOP, 99%), dioctyl sebacate (DOS), AIBN, potassium chloride, ethylenediaminetetraacetic acid (EDTA), sodium hydroxide, calcium chloride, sodium chloride, aluminum chloride, magnesium sulphate, cobalt chloride, nickel chloride, mercuric chloride, lead nitrate, copper sulphate, potassium carbonate and zinc chloride were purchased from Merck.

2.2 Instruments

The structure characterization of the EAAP ligand was performed *via* the ^{1}H NMR spectra (δ, ppm) which were measured on a Bruker Avance III 400 MHz (Faculty of Pharmacy, Mansoura University) using tetramethylsilane (TMS) as an internal reference and using DMSO-d_6 as a solvent. The exchangeable protons were detected through D_2O testing. The multiplicities of the signals were reported as follows: s = singlet, d = doublet, dd = doublet of doublets, t = triplet, and m = multiplet. The electron impact mass spectra (EIMS) were determined on a ThermoFisher Scientific DSQ II GC/MS with focus GC (70 eV) (Faculty of Science, Mansoura University). Elemental analyses (C, H and N) were executed at the microanalytical lab at Cairo University. The

synthesis of the EAAP chelating ligand was monitored using thin layer chromatography (TLC) on aluminum sheets pre-coated with Al_2O_3 with fluorescent indicator F254 (Merck, Darmstadt, Germany). The spots were detected by exposure to a UV lamp at λ = 254 nm. Moreover, the FT-IR spectra (IR) (ν, cm^{-1}) of the synthesized EAAP ligand and the formed polymers were obtained in the range of 400–4000 cm^{-1} using the pressed KBr pellet method on a Mattson 5000 FT-IR spectrophotometer (Faculty of Pharmacy, Mansoura University) and Thermo Fisher Nicolet IS10, USA (Spectral Analytical Unit, Faculty of Science, Mansoura University). In addition, the morphological surfaces and elemental analyses of the polymers were investigated by scanning electron microscopy (QUANTA FEI 450, Netherlands) and energy-dispersive X-ray spectroscopy (X-Max), respectively. For the potentiometric measurements, the modified GCE (working electrode, 3 mm diameter) was connected on a digital pH/mV meter (4120300 JP Selecta, Spain/EU) with a standard calomel electrode (reference electrode) at ambient temperature to form the following cell (calomel electrode | solution | modified GCE). Moreover, the hydrogen ion concentration of the prepared solutions was adjusted by the same pH/mV meter. On the other hand, the Ag/AgCl electrode (reference electrode) was dipped in different solutions with the modified GCE (working electrode) and platinum electrode (auxiliary electrode) to determine the different electrochemical measurements (*e.g.*, electrochemical impedance spectrophotometry (EIS), (CV), (ASV),…*etc.*) by a digital potentiostat (Gamary, Interface 5000E/potentiostat/galvanostat/ZRA).

2.3 Preparation of the EAAP chelating ligand

2.3.1 Ethyl 2-amino-6-hydroxy-4-phenyl-4*H*-benzo[*f*]chromene-3-carboxylate (1). A mixture of 2,7-dihydroxynaphthalene (480 mg, 3 mmol) and ethyl benzylidenecyanoacetate (603 mg, 3 mmol) was refluxed in absolute ethanol (15 mL) in the presence of a catalytic amount of piperidine for 2.5 h. After cooling, the formed precipitate was filtered off and recrystallized from EtOH to yield the product **1** (954 mg, 88%); colorless crystals; m.p. = 208–210 °C; IR (KBr, ν/cm^{-1}): 3474 (OH), 3474 and 3304 (NH_2), 1661 (C=O), 1625 (C=C), 1213 (C–O) (Fig. S1, ESI†); ^{1}H-NMR (400.20 MHz, DMSO-d_6): δ (ppm) = 1.27 (t, 3H, J = 8 Hz, –CH_2CH_3), 4.09 (m, 2H, –CH_2CH_3), 5.29 (s, 1H, H-4), 7.62 (br, 2H, NH_2), 6.95–7.77 (m, 10H, ArH), 9.88 (s, 1H, OH) (Fig. S2, ESI†); (EIMS) m/z (%): 361.1 [M^+] (11.8), 313.1 (1.9), 288.0 (13.8), 285.2 (19.3), 284.0 [M^+–Ph] (100.0), 256.0 (11.6), 238.0 (42.7) (Fig. S3, ESI†); anal. calcd for $C_{22}H_{19}NO_4$ (361.13): C, 73.12; H, 5.30; N, 3.88%. Found: C, 73.29; H, 5.42; N, 3.95%.

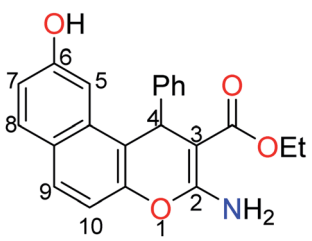

2.3.2 Ethyl 6-(allyloxy)-2-amino-4-phenyl-4*H*-benzo[*f*]chromene-3-carboxylate (2). A mixture of compound **1** (722 mg, 2 mmol), allyl bromide (0.22 mL, 2.6 mmol) and anhydrous K_2CO_3 (1.5 g) in dry acetone (20 mL) was refluxed for 2 h. The reaction was left to cool and filtered off; then, the solvent was removed under reduced pressure. The formed precipitate was washed with 50 mL cold water, filtered off, and then recrystallized from EtOH to afford the desired product **2** (545 mg, 68%); colorless crystals; m.p. = 155–156 °C; IR (KBr, ν/cm^{-1}): 3408 and 3302 (NH_2), 1670 (C=O), 1628 (C=C) (Fig. S4, ESI†); ^{1}H-NMR (400.20 MHz, DMSO-d_6): δ (ppm) = 1.25 (t, 3H, J = 8 Hz, –$CH_2C\underline{H}_3$), 4.10 (m, 2H, –$C\underline{H}_2CH_3$), 4.55 (dd, 1H, J = 4, 12 Hz, CH_2=CHC$\underline{H}_{2a}$–), 4.73 (dd, 1H, J = 4, 12 Hz, CH_2=CHC$\underline{H}_{2b}$–), 5.30 (d, 1H, J = 8 Hz, C$\underline{H}_{2a}$=CHCH_2–), 5.38 (s, 1H, H-4), 5.44 (d, 1H, J = 16 Hz, C$\underline{H}_{2b}$=CHCH_2–), 6.08 (m, 1H, CH_2=C$\underline{H}$CH_2–), 7.05–7.84 (m, 10H, ArH), 7.65 (s, 2H, NH_2) (Fig. S5, ESI†); anal. calcd for $C_{25}H_{23}NO_4$ (401.16): C, 74.80; H, 5.77; N, 3.49%. Found: C, 74.91; H, 5.87; N, 3.60%.

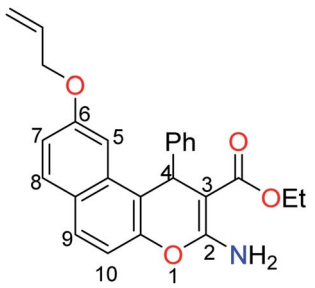

2.4 Preparation of host-tailored polymer

IIP for Cd(II) was fabricated by the thermal polymerization technique. Typically, 2 mmol of EAAP was dissolved in 25 mL aqueous ethanol (50%), then mixed with 1 mmol of Cd(II). The stirring was continued for 30 min at room temperature to induce the formation of a complex between the synthesized ligand and Cd(II). Thereafter, 3 mmol of EGDMA and 0.1 g of AIBN were added to achieve polymerization at room temperature with continuous stirring until homogenized. The mixture was deoxygenated by purging with nitrogen gas for the appropriate time and then polymerized in a water bath at 60 °C for 24 h. After the polymerization step, the cadmium ions were removed from the polymeric matrices using nitric acid (0.1 mol L^{-1}). The complete removal of template ions was checked by UV-Vis analysis at the cadmium absorption peak, λ_{max} = 510 nm. The imprinted polymer was washed with deionized water and left to dry at ambient temperature. In the same way, the corresponding non-imprinted polymer (NIP) was obtained by using the same protocol in the absence of the template ions. Finally, the polymeric membrane was deposited on the surface of GCE for the examination of the potentiometric and voltammetric measurements.

2.5 Sensor construction and electrochemical measurements

The voltammetric sensor was prepared by depositing graphene oxide on GCE after polishing the surface with alumina slurry

(0.05 μm) followed by washing with EtOH and distilled water. Then, the IIP was dropped on GO@GCE and the modified electrode was maintained for 3 h at room temperature. Thereafter, the prepared sensor (IIP/GO@GCE) was characterized by CV and EIS. Under optimized conditions, the IIP/GO@GCE was immersed in a mixture containing 0.1 mol L^{-1} acetate buffer and 5×10^{-5} mol L^{-1} Cd(II) solution for CV investigation (the potential window is from −1.5 V to 1 V, scanning rate: 100 mV s^{-1}). Meanwhile, the EIS analysis was accomplished in the frequency range from 0.1 Hz to 100 kHz in 0.1 mol L^{-1} KCl solution containing 5×10^{-3} mol L^{-1} $Fe(CN)_6^{3-/4-}$ as the redox active probe. The electrochemical detection of Cd(II) was already performed by ASV under optimized conditions (scanning voltage: −1.5–0.1 V, deposition potential: −1.5 V; scan rate: 100 mV s^{-1}; pulse amplitude: 50 mV; pulse width: 50 ms).

On the other hand, the sensing membrane of the potentiometric sensor was synthesized by inserting the prepared polymer in plasticizer and embedding it in the PVC matrix. Briefly, PVC powder (30 mg) was slowly dispersed in 2.5 mL of DMF, followed by addition of IIP (ionophore, 0.01 g) and DOP plasticizer (0.5 mL) with continuous stirring until homogeneity. After polishing the surface of GCE as previously mentioned, it was inserted in the plasticized sensing mixture until it was completely covered with a thin layer, and it was then left to evaporate under air. The modified sensor (IIP/PVC@GCE, working electrode) was connected to a saturated calomel electrode (SCE, reference electrode) at the digital pH/mV meter to form the following electrochemical cell: the developed sensor | sample solution | SCE. For comparison, the non-imprinted sensor (NIP/PVC@GCE) was prepared by the same way using NIP instead of MIP. The electromotive force (EMF) of the proposed sensor was measured for different Cd(II) concentrations after potential stabilization at ±2 mV. The EMF readings were plotted *versus* the logarithm concentration of Cd(II) to acquire the calibration curve. It is worth mentioning that the proposed electrode was stored and conditioned in 1.0×10^{-3} mol L^{-1} Cd(II) solution at pH 4.5 before the electrochemical measurements.

2.6 Sample preparation

2.6.1 Human hair. Scalp hair samples were obtained from a male barbershop in the city of Samannud, Egypt, for the recognition and the determination of Cd(II). To remove fat and other surface contaminations from the hair sample, it was placed in a beaker and then washed with distilled water and acetone. The sample was dried in an oven at 85 °C until a constant weight was obtained. Accurately, 0.1 g portion of the sample was weighed, digested by a mixture solution of concentrated nitric acid and hydrochloric acid, and then heated gently to near dryness, and different drops of concentrated H_2SO_4 were added to the residue. After filtration, the remaining residue was diluted to 100 mL with distilled water. The pH of the solution was adjusted to 4.5 using acetate buffer. As previously mentioned, the concentration of Cd(II) was measured using the proposed sensors by voltammetric and potentiometric methods. The *F*-test and *t*-test were elaborated to compare the precision and the accuracy of both methods.

2.6.2 Blood samples. Five human blood samples were obtained from healthy volunteers. The samples were prepared by centrifugation at 3000 rpm for 15 min to separate the blood serums and maintained for 5 min. For each analysis, 100 μL of serum sample was transferred to the electrochemical cell, which contained 5.0 mL of 0.1 mol L^{-1} acetate buffer (supporting electrolyte) of pH 4.5. Afterwards, the concentration of Cd(II) was evaluated using voltammetric and potentiometric sensors. Furthermore, to assess the reproducibility of the procedures, the serum samples were spiked with various concentrations of Cd(II) and were measured alternately before and after Cd(II) addition using the calibration curve that was obtained under the optimized conditions.

3. Results and discussion

3.1 Preparation and characterization of the EAAP chelating ligand

The treatment of 2,7-dihydroxynapthalene with ethyl benzylidenecyanoacetate in an equimolar ratio under basic conditions afforded the benzo[*f*]chromene **1** in excellent yield (88%) *via* a convenient and high-yielding protocol (Scheme 1).[24] The enaminoester chelation side was characterized using its IR spectrum, which showed the amino group absorption bands at 3410 and 3304 cm^{-1} and the ester C=O stretching band at 1661 cm^{-1}. Moreover, the ^{1}H-NMR spectrum showed a broad singlet at δ 7.62 ppm, which is attributable to the NH_2 group,

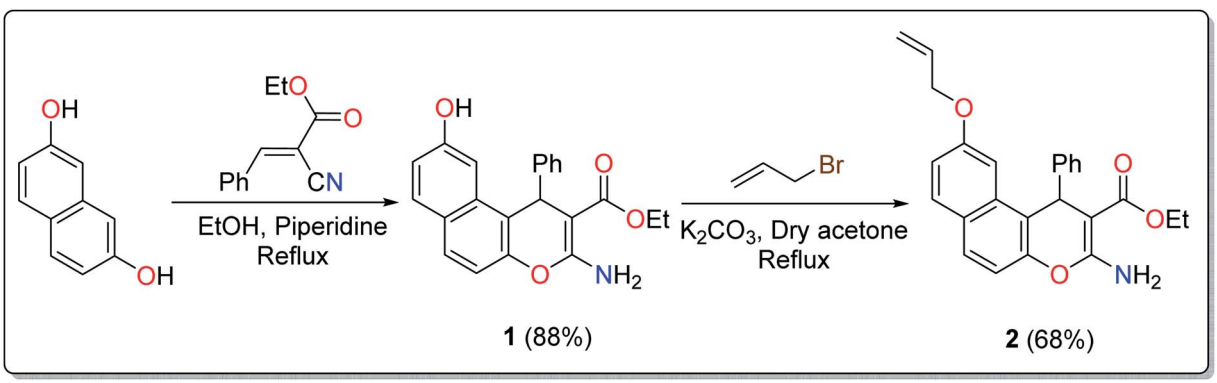

Scheme 1 Synthesis of the EAAP ligand.

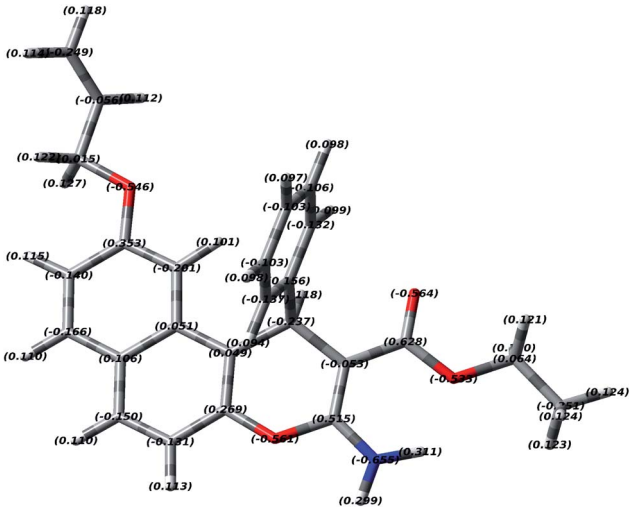

Fig. 1 Electron densities of EAAP based on the DFT studies.

while the signals at δ 1.27 and 4.09 ppm are assignable to the ester methyl and methylene groups, respectively.

The next step involved the insertion of the allyl arm as the root of the polymerization process. The allylation step of the 6-hydroxy-4*H*-benzo[*f*]chromene **1** was accomplished *via* its reaction with allyl bromide in the presence of anhydrous K_2CO_3 to afford the EAAP ligand **1** in good yield (68%).[25]

3.2 DFT study of EAAP

In order to study the most preferred chelation position of the EAAP ligand, the charge densities on the atoms were computationally calculated using the Gaussian 09 software package. The electron densities were measured on the most optimized structure at the DFT level *via* B3LYP as the energy function, 6-31G (d,p) as a basis set and ethanol as a solvent (Fig. 1).[26,27]

It was found that the electron densities of the nitrogen atom (-0.655 e Å^{-3}) and the ester sp^2 oxygen (-0.564 e Å^{-3}) were the highest compared with the other nucleophilic centers present in the ligand. According to this, the chelation direction (A) was excluded because the ester SP^3 oxygen has lower electron density compared with the SP^2 oxygen (Fig. S6, ESI†). Therefore, the chelation direction (B) is predominant, and the cadmium ions will occupy their specific holes according to Scheme 2.

3.3 Characterization of the prepared imprinted polymer

3.3.1 FT-IR spectra. To investigate the chemical modifications throughout the polymerization process, the IR spectra of un-leached IIP, leached IIP and NIP were obtained (Fig. S7, ESI†). The FT-IR bands that appeared in the un-leached polymer at wavenumbers of 3350 cm^{-1}, 2960 cm^{-1} and 1450 cm^{-1} were assigned to NH_2 stretching, C=O stretching and bending, respectively.[28,29] These bands demonstrated the successful insertion of EAAP chelating ligand on the polymeric matrix during the polymerization process. Moreover, the spectrum of leached IIP was approximately analogous to that of NIP, revealing the similarity of their backbone constructions and the complete removal of Cd(II) without affecting the main structure of the polymer.

3.3.2 SEM and EDX analysis of the imprinted polymers of Cd(II). The morphological structures of NIP, un-leached IIP and leached IIP were characterized by SEM (Fig. 2). As can be seen, the roughness and porosity of the surface of IIP increased after leaching the template ions compared to the surface of the NIPs, and un-leached IIP is considered a good indication of successful elaboration of an imprinted polymer.[30] This porosity may facilitate the fast binding of the template ions to the surface of the modified GCE. Moreover, compared with the leached IIP, the presence of cadmium peaks in the EDX analysis of un-leached IIP revealed the successful invasion of Cd(II) in the polymeric matrix (Fig. 3).

3.4 Electrochemical characterization

3.4.1 Analytical features of the sensors. The synthesized IIP and NIP were examined as sensing membranes in the proposed potentiometric sensor (IIP/PVC@GCE). The sensor was characterized as a potentiometric transduction according to the IUPAC guidelines. The electrochemical signals of a conventional design under static conditions are exhibited in Fig. S8 (ESI†). The sensor showed near-Nernstian behavior towards Cd(II), with a cationic slope of 61.4 ± 0.2 (R^2 = 0.96) mV per decade over a linear range of 7.3×10^{-8} mol L^{-1} to 2.4×10^{-3} mol L^{-1} and

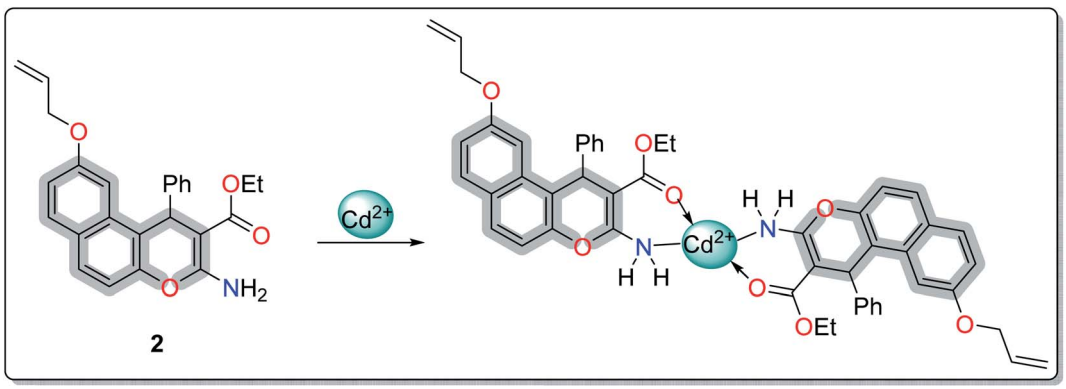

Scheme 2 The preferred chelation direction based on the DFT studies.

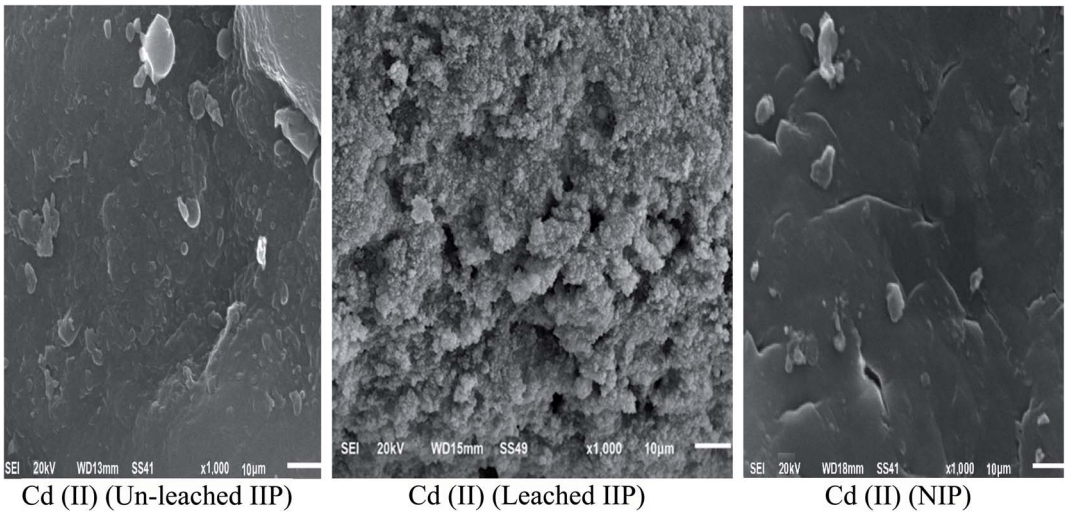

Fig. 2 SEM images of the synthesized un-leached and leached cadmium imprinted polymer and non-imprinted polymer.

a lower detection limit (LOD = 6.3×10^{-10} mol L^{-1}). As a control, the sensor membrane based on NIP showed low response towards Cd(II) when compared with the response of the IIP/PVC@GCE sensor. These results proposed that the recognition of Cd(II) ions was achieved based solely on the tailored cavities on the surface of the polymeric matrix.

Moreover, the reproducibility was examined by recording six measurements for Cd(II) solutions, and the relative standard deviation (RSD) was found to be 2.6%. These results indicate that the proposed sensor has excellent reproducibility. In addition, to determine the stability of this modified electrode, the potentiometric signals were recorded repeatedly for two months and compared with the primary data. There was no observable change in the potentiometric signals after eight weeks.

3.4.2 CV and EIS. The performance and electrochemical behavior of various modified sensors (GCE, GO@GCE, un-leached IIP/GO@GCE, leached IIP/GO@GCE, and NIP/GO@GCE) were investigated using CV and EIS. Therefore, the proposed sensors were introduced in a buffered Cd(II) solution (5.0×10^{-5} mol L^{-1}). As shown in Fig. 4, the anodic and/or cathodic peak current of Cd(II) was elevated dramatically after dropping GO on the GCE surface; this implies that GO has high conductivity and a large surface area, which enhance electron exchange for cadmium ions. Alternatively, a sharp decrease in the peak current intensity was noticed after immobilization of un-leached IIP and/or NIP. This can be attributed to the hindering effect of non-conductive polymers. Meanwhile, after coating GO@GCE with the leached polymer, the peak current was elevated due to the molding of the cavities for Cd(II) ions in the surface of the polymeric matrices during the leaching process, which facilitates the diffusion of cadmium ions from the bulk to the surface of the working electrode.[12,31]

EIS is also a powerful technique, and it was used for investigation of the resistance change using the electrochemical probe ($K_3[Fe(CN)_6]$) at the modified sensor interface. The data

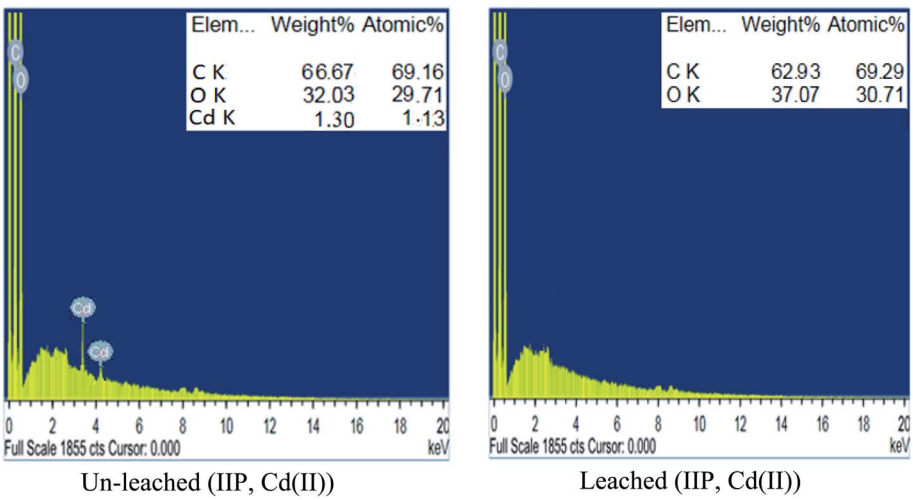

Fig. 3 Energy-dispersive X-ray analysis images of un-leached and leached IIP for the Cd(II) template.

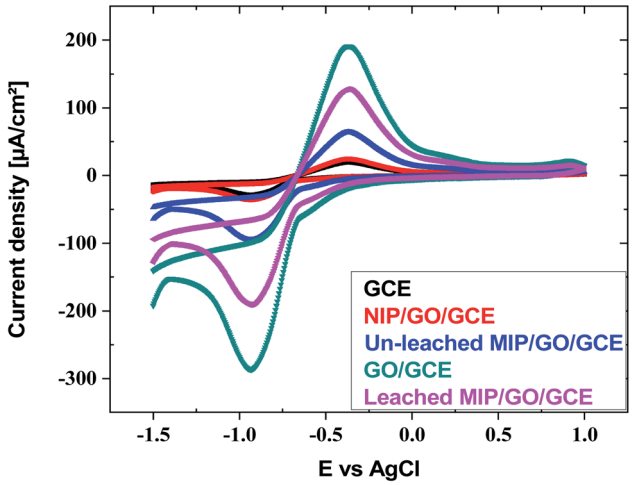

Fig. 4 Cyclic voltammograms of GCE, GO@GCE, NIP/GO@GCE, un-leached IIP/GO@GCE and leached IIP/GO@GCE in Cd(II) solution buffered with acetate.

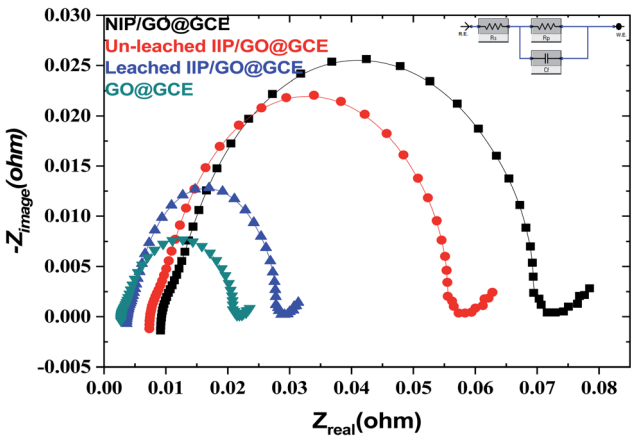

Fig. 5 EIS of GC, GO@GCE, NIP/GO@GCE, un-leached IIP/GO@GCE and leached IIP/GO@GCE in a solution of 5.0×10^{-3} mol L^{-1} $[Fe(CN)_6]^{3-/4-}$ and 0.1 mol L^{-1} KCl.

presented in Fig. 5 show the variation in the polarization resistance (R_p) for the proposed sensors based upon the variance of the semicircle diameter. Compared with the GO@GCE, the un-leached IIP/GO@GCE and NIP/GO@GCE displayed larger circular radii, which confirmed that the proposed polymers were non-conductive materials. Meanwhile, the R_p dramatically decreased when the un-leached IIP was replaced with leached IIP; this was attributed to the formation of some channels and cavities on the IIP film, which facilitated the penetration of the probe.

3.5 Optimization of the work conditions

3.5.1 Effect of pH. The pH of the supporting electrolyte influences not only the rate of electron transfer, but also the rebinding of the Cd(II) ions template with the polymeric matrix on the electrode surface. Consequently, the effect of hydrogen ion concentration was studied by evaluating the CV and ASV voltammograms of the voltammetric sensor in 5.0×10^{-5} mol L^{-1} Cd(II) ions buffered at different pH values (Fig. S9, ESI†). It was noted that the peak potential shifted negatively with increasing pH value. Moreover, the peak current of the ASV increased gradually and reached its maximum at pH 4.5, which was chosen as an optimum pH in the other experimental studies. As the pH increased, the peak current decreased; this is possibly owing to the formation of precipitation ($Cd(OH)_2$) due to the lower value of K_{sp} (7.2×10^{-15}).

On the other hand, for a potentiometric sensor, a great effect on the potential responses was observed when the pH of the solution was varied (Fig. S10, ESI†). As expected, the potential was elevated regularly and reached its maximum at pH 4.5. Thus, pH 4.5 was selected as the optimum value.

3.5.2 Effect of the response time and reversibility of potentiometric sensor. The response time is the average time which is required to reach a steady state potential (±3 mV) using the potentiometric sensor in the range from 7.3×10^{-8} to 2.4×10^{-3} mol L^{-1} Cd(II) solution with a fast ten-fold accretion in concentration. As exhibited in Fig. S11 (ESI†), the response time of IIP/PVC@GCE was noted to be less than 5 s. This result indicates that the potentiometric sensor can overcome the memory effect and rapidly reach equilibrium.

3.5.3 Selection of the washing solvent and the effect of leaching time. For regeneration of the sensors, the cadmium ions which are detected by the modified GCE should be eluted after each detection. Thus, nitric acid, EDTA, hydrochloric acid and sodium hydroxide were tested for removal of the cadmium template. The complete removal of Cd(II) ions was achieved by using nitric acid (0.1 mol L^{-1}) for both electrochemical sensors. Furthermore, it was noted that the electrochemical signals of both sensors varied with increasing leaching time. The peak current of the voltammetric sensor was elevated with increasing leaching time and reached the maximum at 90 s for Cd(II) (Fig. S12, ESI†). Meanwhile, the signals of the potentiometric sensor increased gradually with the elution time up to 60 s for Cd(II).

3.5.4 Effect of the scan rate for the voltammetric measurements. The electrochemical behavior of 5×10^{-5} mol L^{-1} Cd(II) at IIP/GO@GCE was evaluated by CV in acetate buffer (pH 4.5) at different potential scan rates from 10 mV s^{-1} to 250 mV s^{-1}. It was observed that increasing the scan rate shifted the peak current toward a positive direction

Table 1 The selectivity coefficients of the potentiometric sensors

Interferent	Cd(II)	Ni(II)	Co(II)	Pb(II)	Cu(II)	Mg(II)	Hg(II)	Ca(II)	Zn(II)
log $K_{Cd(II),i}$ IIP/PVC@GCE	—	−2.6	−1.9	−0.9	−1.8	−2.9	−1.3	−2.8	−1.7

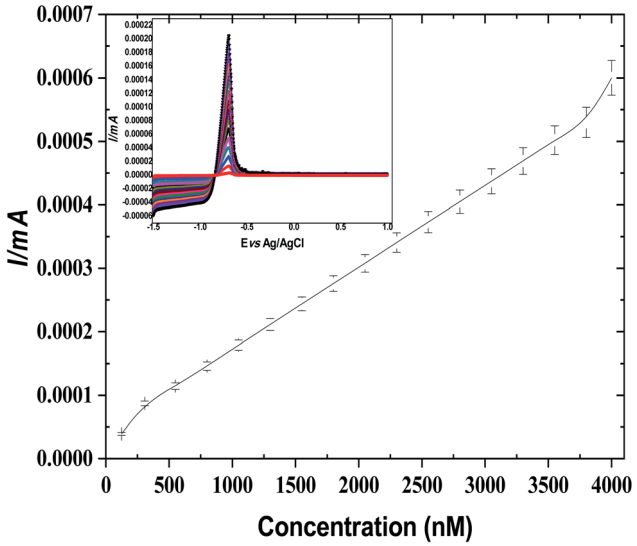

Fig. 6 The anodic stripping voltammetry of the IIP/GO@GCE sensor in different concentrations of Cd(II). Deposition potential: −1.5 V; scan rate: 100 mV s^{-1}; pulse amplitude: 50 mV; pulse width: 50 ms.

and that the magnitude value was elevated gradually, which indicated that the electrochemical reaction was predominantly controlled by the diffusion process (Fig. S13, ESI†). Furthermore, it was noted that the peak potential (E_{pa}) was directly proportional to log ν (Fig. S14, ESI†) and the linear regression equations can be expressed as follows:

$$E_{p,a}(mV) = 0.18 \log \nu + 1.14 \ (R^2 = 0.99)$$

In addition, the value of the electron transfer for an oxidation–reduction reaction can be calculated using the Tafel equation, and it was equal to 2.[32]

3.5.5 The interference and the selectivity of the proposed electrodes. To assess the selectivity of both electrochemical sensors for the Cd(II) template, Ni(II), Co(II), Pb(II), Cu(II), Mg(II), Hg(II), Ca(II), and Zn(II) were chosen as the analogues that affect the recognition and detection of Cd(II). The anodic peak current of Cd(II) ion was much higher than that of the interfering ion peaks, which can be attributed to the incompatibility of the cavities in the polymeric matrix with the other interfering ions (Fig. S15, ESI†). In addition, the data indicated that a 200-fold concentration of the interfering ions significantly affects the intensity of the ASV of cadmium. Also, the imprinting factor (the ratio of the peak current between the imprinted sensor and the non-imprinted sensor to Cd(II)) equaled 7.7.[33]

Table 2 Recovery% of Cd(II) from human blood samples and scalp hair samples using the voltammetric and the potentiometric sensors

Sample	Cd(II) added (μM)	Cd(II) founded by voltammetric sensor[a] (μg)	Recovery%	Cd(II) founded by potentiometric[a] (μg)	Recovery%	*F*-test	*t*-test
Person 1	0	1.7 ± 0.11	—	1.76 ± 0.13	—	1.39	1.2
	5	6.6 ± 0.09	98.5	6.58 ± 0.12	99.6	1.77	1.6
	10	11.72 ± 0.2	100.1	11.69 ± 0.22	99.4	1.21	1.54
Person 2	0	1.53 ± 0.13	—	1.52 ± 0.1	—	1.69	0.8
	5	6.5 ± 0.16	99.5	6.43 ± 0.2	98.6	1.56	1.2
	10	11.55 ± 0.18	100.17	11.5 ± 0.23	99.8	1.6	1.3
Person 3	0	1.5 ± 0.05	—	1.6 ± 0.07	—	1.96	0.7
	5	6.45 ± 0.11	99.2	6.49 ± 0.14	98.3	1.6	1.4
	10	11.48 ± 0.2	99.8	11.45 ± 0.25	98.7	1.56	1.5
Person 4	0	1.81 ± 0.06	—	1.79 ± 0.09	—	2.25	—
	5	6.8 ± 0.1	99.8	6.9 ± 0.11	101	1.21	1.3
	10	11.79 ± 0.17	99.8	11.8 ± 0.23	100	1.8	1.2
Person 5	0	1.4 ± 0.1	—	1.46 ± 0.1	—	1	0.9
	5	6.4 ± 0.12	100	6.42 ± 0.15	99.3	1.56	1.2
	10	11.35 ± 0.16	99.5	11.39 ± 0.19	99.4	1.4	1.4
Human hair 1	0	2.6 ± 0.18	—	2.71 ± 0.2	—	1.23	1.8
	5	7.5 ± 0.15	98.6	7.6 ± 0.18	98.5	1.44	1.1
	10	12.62 ± 0.2	100.15	12.65 ± 0.21	99.5	1.1	1.6
Human hair 2	0	2.59 ± 0.13	—	2.61 ± 0.1	—	1.69	1.8
	5	7.6 ± 0.18	100.13	7.6 ± 0.14	99.8	1.65	1.5
	10	12.55 ± 0.3	99.6	12.57 ± 0.23	99.7	1.7	1.9
Human hair 3	0	2.9 ± 0.1	—	3.1 ± 0.14	—	1.96	0.7
	5	7.86 ± 0.24	99.4	8 ± 0.19	98.7	1.59	1.5
	10	13 ± 0.19	100.7	12.9 ± 0.26	98.4	1.87	1.6
Human hair 4	0	3.4 ± 0.16	—	3.51 ± 0.12	—	1.77	0.9
	5	8.41 ± 0.22	100.1	8.48 ± 0.21	99.6	1.09	1.1
	10	13.38 ± 0.19	99.8	13.46 ± 0.23	99.6	1.46	1.6
Human hair 5	0	3.2 ± 0.07	—	3.1 ± 0.1	—	2.04	1.3
	5	8.1 ± 0.13	98.7	7.9 ± 0.16	97.5	1.5	0.8
	10	13.3 ± 0.23	100.7	13 ± 0.24	99.2	1.08	1.1

[a] Mean values with RSD.

On the other hand, by using the fixed interference method (FIM), the selectivity of the potentiometric sensor was checked. The selectivity coefficients (the ratio of the activity between Cd(II) (primary ion) and the interfering ion powered by their charges) were estimated by using 1.0×10^{-2} mol L^{-1} of the interfering ions. The selectivity coefficients of the synthesized sensor over various, relevant ions, such as Ni(II), Co(II), Pb(II), Cu(II), Mg(II), Hg(II), Ca(II), and Zn(II), are summarized in Table 1. It is worth mentioning that the existence of a 100–150 fold excess of different inorganic cations did not interfere in the performance of IIP/PVC@GCE.

Furthermore, in the comparison with NIP/PVC@GCE, the proposed imprinted sensor showed excellent selectivity toward Cd(II) compared to the interfering ions (Table S2, ESI†). These results can be attributed to the selective attraction of Cd(II) ion to its specific holes in the surface of the imprinted polymer.

3.5.6 Effects of the deposition potential and deposition time on ASV. The deposition potential and deposition time are the most critical parameters that affect the sensitivity and the selectivity of the anodic stripping voltammetry technique. The negative deposition potential is typically related to the standard reduction potential to reduce the target ions on the working electrode surface to atoms. Therefore, the potential of deposition was studied in the range from −1.9 V to −0.9 V. The optimum deposition potential was selected at −1.5 V, which represented the maximum value of the current intensity as shown in Fig. S16 (ESI†).

It is worth mentioning that at more negative potential, the reduction of hydrogen becomes a significant issue due to formation of hydrogen bubbles at the modified GCE surface. According to the aforementioned, the reduced stripping signals may affect the selectivity of the proposed electrode. Moreover, in order to enhance the sensitivity of modified GCE, the deposition time was tested in the range from 20 to 100 s (Fig. S17, ESI†). It was observed that increasing the deposition time enabled more cadmium atoms to be deposited at the modified GCE surface. However, the current signals became almost constant after 60 s, which can be attributed to saturation of GCE surface by the cadmium metal.

Furthermore, for comparison, ASV was investigated for Cd(II) by using bare GCE, GO@GCO, NIP/GO@GCE, and leached and un-leached IIP/GO/GCE. As exhibited in Fig. S18 (ESI†), the peak current intensity of GO@GCE is higher than that of the other corresponding sensors due to the high conductivity and the large surface area of the GO. In contrast, the non-imprinted sensor (NIP/GO/GCE) and the un-leached IIP/GO@GCE sensor displayed lower responses toward cadmium ions. Meanwhile, in leached IIP/GO@GCE, the current intensity elevated rapidly; this contributed to the formation of some channels on the imprinted film, which facilitated the penetration of the cadmium template from the bulk to the GCE surface.

3.5.7 The analytical features. Under optimal experimental conditions, the peak current of ASV presented a linear relationship with the corresponding cadmium concentrations in the range from 4.2×10^{-12} to 5.6×10^{-3} mol L^{-1} (Fig. 6), based on the following equation:

$$I = 0.6C \text{ (mol L}^{-1}\text{)} + 2.4 \times 10^{-3} \ (R^2 = 0.99)$$

Based on the calculation results, the limit of detection and limit of quantification of the voltammetric sensor can reach 7×10^{-14} mol L^{-1} and 2.33×10^{-13} mol L^{-1}, respectively. In contrast, the electrochemical signals of the potentiometric sensor were directly proportional to the Cd(II) concentration in the range from 7.3×10^{-8} mol L^{-1} to 2.4×10^{-3} mol L^{-1}, with a lower detection limit of 6.3×10^{-10} mol L^{-1}.

The stability and reproducibility are also crucial parameters for the assessment of the proposed sensors. To evaluate the reproducibility, the voltammetric electrode at different concentrations of Cd(II) ions was examined by the ASV technique in the presence of acetate buffer (pH 4.5). Well-shaped voltammograms were acquired for the experiments: the relative standard deviation (RSD) for the slopes was 2.4%. Moreover, the peak signal of the cadmium voltammetric sensor was reduced to 89% of the original value after 30 days. Moreover, the performance criteria of the fabricated sensor (IIP/GO@GCE) were compared with those of other electrochemical methods for cadmium determination by voltammetric techniques, and the corresponding results are summarized in Table S1 (ESI†). Compared with the potentiometric sensor, a high linear concentration range, excellent stability and a low detection limit were noted for IIP/GO@GCE; all of these characteristics make it a great promising sensor in the electro-analysis of Cd(II).

3.5.8 Analytical application. To evaluate the applicability of the voltammetric and the potentiometric sensors, the concentration of Cd(II) solution was detected in various biological samples (blood serum samples and human hair samples). Both sensors were inserted directly into the prepared samples; the observed signals were evaluated and compared with the calibration plot, and the output readings are listed in Table 2. Excellent recoveries were noted in the determination of Cd(II) that ranged from 98.3% to 101%, and the RSD values were less than 4%. Moreover, according to the *F*-test and *t*-test, there is no significant difference between the analysis results of the proposed methods using IIP/GO@GCE and those using IIP/PVC@GCE.

4. Conclusions

In summary, highly selective and sensitive electrochemical sensors were used for the recognition of cadmium ions in different biological samples based on a promising enaminoester ligand. The voltammetric sensor was fabricated based on modification of GCE with GO and IIP. In contrast, polyvinyl chloride and the prepared polymer were utilized to perform the potentiometric sensing. Compared with IIP/PVC@GCE, a high linear concentration range (4.2×10^{-12}–5.6×10^{-3} mol L^{-1}), low detection limit (7×10^{-14} mol L^{-1}), good reproducibility (2.4%), and excellent stability (30 days) were observed for IIP/GO@GCE. In addition, the proposed sensors displayed good recognition capacity for cadmium ions over other structurally similar ions. Furthermore, both sensors were successfully applied for trace Cd(II) detection in real samples with acceptable recoveries (98.3–101%). Due to the abovementioned merits, our

developed sensors are expected to be promising for electrochemical applications.

Ethical statement

All experiments were performed in accordance with the ethical rules approved by the ethics committee at the Faculty of Science, Mansoura University. The institution approval code is SCI-Ch-P-2021-126. In addition, informed consent was obtained from the human participants of this study.

Conflicts of interest

There are no conflicts to declare.

Acknowledgements

The authors are grateful for the Mansoura University Sustainable Energy Research lab (MSER) which supported by the Science, Technology & Innovation Funding Authority (STDF).

References

1 Y. Li, Y.-s. Huang, B. He, R. Liu, G. Qu, Y. Yin, J. Shi, L. Hu and G. Jiang, *Ecotoxicol. Environ. Saf.*, 2020, **188**, 109896.
2 S. M. Prabu, K. Shagirtha and J. Renugadevi, *J. Food Sci.*, 2010, **75**, T132–T140.
3 S. Satarug, J. R. Baker, S. Urbenjapol, M. Haswell-Elkins, P. E. Reilly, D. J. Williams and M. R. Moore, *Toxicol. Lett.*, 2003, **137**, 65–83.
4 C. A. Rusinek, A. Bange, I. Papautsky and W. R. Heineman, *Anal. Chem.*, 2015, **87**, 6133–6140.
5 M. Ebrahimi, N. Khalili, S. Razi, M. Keshavarz-Fathi, N. Khalili and N. Rezaei, *J. Environ. Health Sci. Eng.*, 2020, **18**, 335–343.
6 G. Genchi, M. S. Sinicropi, G. Lauria, A. Carocci and A. Catalano, *Int. J. Environ. Res. Public Health*, 2020, **17**, 3782.
7 C. Liu, Y. Zhu, Z. Lu, W. Guo, B. Tumen, Y. He, C. Chen, S. Hu, K. Xu and Y. Wang, *Int. J. Environ. Res. Public Health*, 2020, **17**, 138.
8 V. Zarezade, M. Behbahani, F. Omidi, H. S. Abandansari and G. Hesam, *RSC Adv.*, 2016, **6**, 103499–103507.
9 S. Himeno, E. Kitano and K. Morishita, *Anal. Sci.*, 2007, **23**, 959–962.
10 J. Jiang, Z. Li, Y. Wang, X. Zhang, K. Yu, H. Zhang, J. Zhang, J. Gao, X. Liu and H. Zhang, *Food Chem.*, 2020, **310**, 125824.
11 R. Sun, G. Ma, X. Duan and J. Sun, *Spectrochim. Acta, Part B*, 2018, **141**, 22–27.
12 M. E. Khalifa and A. Abdallah, *Biosens. Bioelectron.: X*, 2019, **2**, 100027.
13 T. Alizadeh, F. Atashi and M. R. Ganjali, *Talanta*, 2019, **194**, 415–421.
14 A. Abdallah, A. El-Shafei and M. E. Khalifa, *Arabian J. Sci. Eng.*, 2021, 1–11.
15 R. F. Aglan, M. M. Hamed and H. M. Saleh, *J. Anal. Sci. Technol.*, 2019, **10**, 1–11.
16 M. H. Mashhadizadeh, K. Eskandari, A. Foroumadi and A. Shafiee, *Electroanalysis*, 2008, **20**, 1891–1896.
17 T. Alizadeh, M. R. Ganjali, P. Nourozi, M. Zare and M. Hoseini, *J. Electroanal. Chem.*, 2011, **657**, 98–106.
18 J. Wang, J. Hu, S. Hu, G. Gao and Y. Song, *Sensors*, 2020, **20**, 1004.
19 S. Hu, G. Gao, Y. Liu, J. Hu, Y. Song and X. Zou, *Int. J. Electrochem. Sci.*, 2019, **14**, 11714–11730.
20 S. D. Masi, A. Pennetta and C. Malitesta, *Proceedings*, 2020, **60**, 39.
21 S. Rais, A. Islam, I. Ahmad, S. Kumar, A. Chauhan and H. Javed, *Food Chem.*, 2021, **334**, 127563.
22 T. K. Biswas, M. M. Yusoff, M. S. Sarjadi, S. E. Arshad, B. Musta and M. L. Rahman, *Sep. Sci. Technol.*, 2021, **56**, 671–680.
23 M. Shamsipur, L. Samandari, L. Farzin and A. Besharati-Seidani, *Microchem. J.*, 2021, **160**, 105714.
24 H. Radwan, H. El-Mawgoud, F. El-Mariah, A. El-Agrody, A. Amr, M. Al-Omar and H. Ghabbour, *Russ. J. Gen. Chem.*, 2020, **90**, 299–304.
25 M. A. Abozeid, M. R. El-Kholany, A.-R. H. Abdel-Rahman and E.-S. I. El-Desoky, *Int. J. Mod. Org. Chem.*, 2018, **5**, 1–11.
26 M. Frisch, G. Trucks, H. Schlegel, G. Scuseria, M. Robb, J. Cheeseman, G. Scalmani, V. Barone, B. Mennucci and G. Petersson, *Gaussian 09, Revision D.01*, Gaussian, Inc., Wallingford, CT, 2009.
27 N. Godbout, D. R. Salahub, J. Andzelm and E. Wimmer, *Can. J. Chem.*, 1992, **70**, 560–571.
28 Y. Wang, E. Wang, Z. Wu, H. Li, Z. Zhu, X. Zhu and Y. Dong, *Carbohydr. Polym.*, 2014, **101**, 517–523.
29 E. Pretsch, P. Bühlmann, C. Affolter, E. Pretsch, P. Bhuhlmann and C. Affolter, *Structure determination of organic compounds*, Springer, 2000.
30 M. E. Khalifa, I. M. Kenawy, Y. Abou El-Reash and A. Abdallah, *J. Environ. Chem. Eng.*, 2017, **5**, 3447–3454.
31 H. da Silva, J. G. Pacheco, J. M. Magalhães, S. Viswanathan and C. Delerue-Matos, *Biosens. Bioelectron.*, 2014, **52**, 56–61.
32 Y. Wang, L. Wang, H. Chen, X. Hu and S. Ma, *ACS Appl. Mater. Interfaces*, 2016, **8**, 18173–18181.
33 B. Deiminiat, G. H. Rounaghi and M. H. Arbab-Zavar, *Sens. Actuators, B*, 2017, **238**, 651–659.